Food Science and Biotechnology (2024) 33:1871–1883
https://doi.org/10.1007/s10068-023-01487-8

RESEARCH ARTICLE

Facile preparation of pH-responsive antimicrobial complex and cellulose nanofiber/PVA aerogels as controlled-release packaging for fresh pork

Tianmeng Hou[1] · Feijie Wang[1] · Liqiang Wang[1]

Received: 11 August 2023 / Revised: 2 November 2023 / Accepted: 14 November 2023 / Published online: 22 December 2023

Abstract
Intelligent controlled release technologies that rely on environmental changes to control the release rate of antimicrobial agents have attracted attention in the field of food preservation. In this paper, cinnamaldehyde (CN) was grafted onto chitosan (CS) to form a pH-responsive controlled-release complex, CS–CN, via the Schiff base reaction. Then, tempo oxidized cellulose nanofibers (CNF) and PVA were prepared as aerogels loaded with CS–CN with different pore parameters (PCNF@CN). Release experiments showed that acid triggered the release of CN and increased the release from 10.3 to 68.4% with increasing pH. In addition, PCNF@CN showed significant pH-responsive antimicrobial properties against *Escherichia coli* and *Staphylococcus aureus*. Utilizing the water absorption of the aerogel and triggering the release of CN, the shelf life of fresh meat could be delayed for 4 days. This study demonstrated the potential application of PCNF@CN aerogel in functional food preservation packaging.

Keywords pH-responsive packaging · Controlled release · Schiff base · Aerogel · Antibacterial

Introduction

The addition of antimicrobial agents to food packaging has been shown to inhibit the growth of microorganisms and extend the shelf life of food. Many studies have proved that the release rate can be controlled by means of micron or nano-encapsulation to achieve a long-lasting antimicrobial effect (Cui et al., 2023). However, the release of antimicrobial agents in packaging is still dependent on their diffusion in the packaging medium rather than release through environmental response. Intelligent controlled-release packaging based on environmental response can trigger the release of the active substance through changes in the microenvironment formed by the food and the package. Therefore, it can slow down the unnecessary loss of volatile antimicrobial agents due to volatilization or early release during storage and distribution.

Imine bonds, also known as Schiff base structures, are dynamic acid-sensitive chemical bonds that are usually formed by condensation reactions between aldehydes and ketones and polymers containing amino groups (Wang et al., 2022a, 2022b). Imine bonds can remain stable in a moderately basic environment but are sensitive to acidity and susceptible to hydrolysis. Chitosan (CS) is rich in amino groups that can undergo Schiff base reactions. Synthesis of pH-responsive controlled-release materials based on CS has been extensively studied in the pharmaceutical field (Xu et al., 2019). In the food industry, several researchers have synthesized pH-responsive CS films containing imine bonds from antimicrobial agents containing aldehyde groups at the solid–liquid interface or inhomogeneous liquid media (Chabbi et al., 2020; Heras-Mozos et al., 2022). However, the hydrophilic nature of CS leads to poor water resistance and mechanical properties of this packaging material, which limits its application in food packaging. Cinnamaldehyde (CN) is an antimicrobial agent of natural origin and contains an aldehyde functional group that can react with the amino

✉ Liqiang Wang
wlqcom@jiangnan.edu.cn

Tianmeng Hou
6210810010@stu.jiangnan.edu.cn

Feijie Wang
7220809010@stu.jiangnan.edu.cn

[1] Jiangsu Provincial Key Laboratory of Food Advanced Manufacturing Equipment Technology, School of Mechanical Engineering, Jiangnan University, Wuxi 214122, China

group of CS to form dynamic imine bonds. On the one hand, it allows to anchor CN on the CS molecules to prevent volatilization and photo-thermal oxidation; on the other hand, the acid-sensitive property of the imine bond can realize the pH-responsive release of CN. pH has a significant impact on the quality of some food products such as fresh meat. Triggering the release of antimicrobial agent based on pH can have the advantage of on-demand release, which is of great significance for the food industry.

Nanocellulose-based aerogel is a biocompatible, low-density porous material (Long et al., 2018). Taking advantages of its excellent properties and adjustable porous structure, it can adsorb moisture and load active substances such as antimicrobial agents and antioxidants for fresh and agricultural products' preservation packaging (Rincón et al., 2023; Wu, 2022).

In this study, a pH-responsive release controller CS–CN was synthesized by grafting CN onto CS via Schiff base reaction, and then CS–CN was loaded into the composite aerogel prepared by tempo-oxidized cellulose nanofiber (CNF) and Polyvinyl alcohol (PVA). The pore parameters of the aerogel were regulated by changing the addition of PVA to make the porous structure of the aerogel more stable and denser. The aerogel mat was subsequently applied to fresh meat preservation to inhibit microbial growth by absorbing juices and triggering CN release. This study provides an effective strategy for pH-responsive release of antimicrobial agents, which has potential applications in the field of intelligent food antimicrobial preservation.

Materials and methods

CS (deacetylation degree of 90%, 150 kDa) was purchased from Zhejiang Golden-Shell Co., Ltd. (Zhejiang, China). CN and PVA were purchased from Macklin Co., Ltd. (Shanghai, China). CNF was provided by Tianjin Woodelf Biotechnology Co., Ltd. (Tianjin, China). Citric acid, Na_2HPO_4, KH_2PO_4, $NaHCO_3$, Na_2CO_3 were obtained from Shanghai Aladdin Biochemical Technology Co., Ltd. (Shanghai, China) to prepare buffer saline.

Preparation of CS–CN

A facile one-pot method was used to synthesize CS–CN. Appropriate improvements were made to the method of Heras-Mozos et al. (2022). 3 g of CS was placed in a conical flask with aldehyde ethanol solution in a ratio of 1:3 (CS:CN). The dosing was carried out according to the molar ratio of repeating units to aldehyde functional groups in CS. Subsequently, the conical flask was kept under agitation in a water bath at 60 °C for 24 h. After extraction, 75 mL of anhydrous ethanol was re-added for shaking and stirring to remove the unreacted aldehyde, and the above process was repeated three times within 24 h. Finally, the samples were dried overnight in an oven at 60 °C to obtain the slight yellow CS–CN.

Preparation of CNF/PVA aerogel

CNF/PVA aerogels were prepared in reference to the method of Zhou et al. (2019). 10 g CNF (1.2%wt) suspension was weighed and diluted. PVA solutions of 1%wt, 3%wt and 5%wt were dispensed and magnetically stirred at 90 °C for 3 h. After cooling to room temperature, added 10 mL of PVA solution to the CNF suspensions separately and stirring to homogenize the suspensions. 350 mg of CS–CN was added to above suspensions to stir well. Finally, 3 mL of suspension was poured into a mold and freeze-dried to obtain P1CNF@CN, P3CNF@CN and P5CNF@CN, respectively. Aerogels without PVA (P0CNF@CN) or CS–CN(PCNF) were prepared with deionized water instead of PVA, and other processes were the same as above. The preparation flow chart of CS–CN and aerogel was shown in Fig. 1.

Characterization of CS–CN

Fourier-transform infrared spectroscopy (FT-IR)

FT-IR spectra of CS, CS–CN were scanned using the Fourier transform infrared spectrometer (Nicolet iS10, Thermo Nicolet Ltd., USA) in the range of 500–4000 cm^{-1} at a resolution of 4 cm^{-1} to analyze the chemical structures of samples.

X-ray diffraction (XRD)

The crystalline shapes of CS and CS–CN were examined using an X-ray diffractometer (D2 Phaser, Bruker AXS, Germany). The samples were scanned at an angle 2θ from 5° to 60° in steps of 5°/min, with Cu-Kα radiation at 40 kV and 30 mA.

Particle size

To obtain the particle size distribution of CS and CS–CN, samples were measured with the laser particle size analyzer (Master Sizer 200, Malvern, UK).

Elemental analysis

The specific test was performed by an elemental analyzer (Vario MACRO Cube, Elementar, Germany) to obtain the content of C, H, and N elements in the particles. The *DS* of CS–CN was calculated according to Eq. 1.

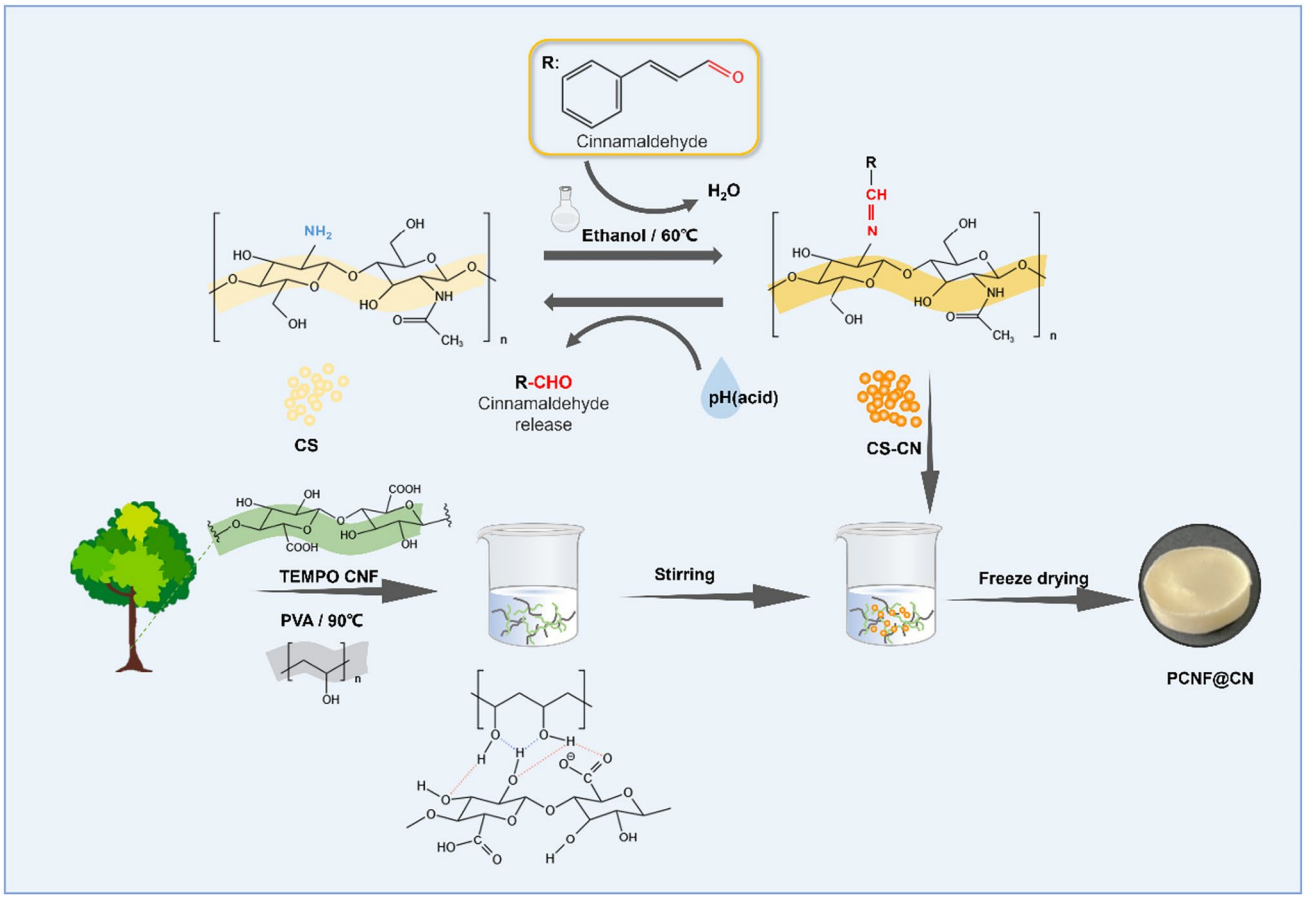

Fig. 1 The preparation flow chart of CS–CN and aerogel

$$DS = \frac{M_n R - (8 - 2DD)M_C}{N_C M_C} \quad (1)$$

Here, DD is the degree of deacetylation of CS; M_C and M_n are the relative atomic masses of carbon and nitrogen atoms, respectively; N_C is the number of carbon atoms in the substituent molecule; R is the percentage ratio of carbon and nitrogen content in CN.

Scanning electron microscopy (SEM)

The surface morphology of CS and CS–CN was observed by scanning electron microscopy (SU1510, Hitachi, Japan) at an accelerating voltage of 10.0 kV. Samples were fixed on the conductive adhesive and sprayed with gold before observation.

UV spectroscopy of CS–CN

The UV absorption properties of the samples were tested referring to Zhu et al. (2023). CS, CS–CN, and CN were dissolved in phosphate-citrate buffer solution at pH 3 (0.5 mg/mL), respectively. A blank buffer without any sample was used as a control. The absorption curves of the above solutions were scanned using a UV spectrophotometer (UV1800, Shimadzu, Japan), ranging from 200 to 800 nm.

To scan the UV spectroscopy of CS–CN in buffers at different pH, CS–CN was added to the buffer solution at pH 3, 5, 7, and 9, respectively (0.5 mg/mL). After 24 h, the UV–Vis spectra curves of CS–CN between 200 and 800 nm were measured.

pH-responsive release and release stability of CS–CN

The release of CN from CS–CN was evaluated under acidic (pH 3 and 5), neutral (pH 7), and alkaline conditions (pH 9). A certain amount of CS–CN was added to the buffer system (0.1 mg/mL) separately. At certain time intervals, 0.2 mL of the release solution was taken for dilution and the absorbance of the liquid at 291 nm was determined using a UV spectrophotometer. And the cumulative release of CN was calculated using the standard curve of the measured CN in each pH buffer.

To study the stability of CS–CN, prepare solution containing CS–CN at different pH (0.1 mg/mL). The absorbance of CS–CN after 8 h release was measured at intervals of 40 days in storage and calculated the amount of CN released.

Characterization of aerogel

FT-IR of aerogel

The aerogels loaded with CS–CN were scanned using FT-IR spectroscopy. The parameter settings were the same as the test for CS–CN.

Morphologies and structural characteristics of aerogels

The surface morphology of CNF/PVA aerogels was examined using SEM. All aerogels were cooled in liquid nitrogen in advance.

The diameter, height, and mass of aerogel were measured by Vernier calipers and analytical balance scale, respectively, and then calculated the bulk density of aerogel.

The porosity of aerogels was carried out referring to Jose et al. (2022).

Mechanical properties of aerogel

The deformation process of aerogels under pressure was measured by using a universal testing machine (E43-104, MTS, China). The compression speed was set to 12 mm/min, and the maximum strain rate was 70%, and then obtained the stress–strain curves.

Release of CN from aerogels and kinetic analysis

The release of CN from the aerogels was determined by UV spectrophotometry (UV1800, Shimadzu, Japan). Added the aerogels into 10 mL buffers of pH 3, 5, and 7, respectively and the absorbance of the solutions was measured at 291 nm at regular intervals. Calculated the cumulative release of CN by the standard curve. Each group of samples was tested three times and the average value was taken.

The data obtained in the above release experiments were fitted with first-order kinetic model (Eq. 2), Higuchi model (Eq. 3), and Korsmeyer–Peppas model (Eq. 4) (Jabbari-Gargari et al., 2022) to investigate the mechanism of CN release from the aerogels.

$$M_t = M_{\max} \times \left(1 - e^{-kt}\right) \tag{2}$$

$$M_t = k_H \times t^{1/2} + b \tag{3}$$

$$M_t = k \times t^n \tag{4}$$

Here, M_t is the cumulative release of CN at time t; M_{max} is the maximum percentage of release; k_H is the dissolution constant; k and n are the release rate and release index, respectively.

Antimicrobial effect of aerogels

Escherichia coli and *Staphylococcus aureus* grow well under weakly acidic to neutral conditions but are inhibited at lower pH (pH < 4) (Valero et al., 2009). Therefore, in order to exclude the effect of strong acids on bacterial growth, the inhibitory effect of different aerogels on *E. coli* and *S. aureus* was determined at pH 5 and 7, with reference to the methods of Meng et al. (2023). Different aerogels with CS or CS–CN were added to bottles containing 9 mL of sterile PBS solution at pH 5 and 7, and then 1 mL of *E. coli* and *S. aureus* bacterial solutions cultured to 10^8 CFU/mL, respectively, and incubated at 37 °C for 24 h. Subsequently, plates were inoculated with a series of 1:10 gradient dilutions of the solutions, and placed in an incubator (37 °C, 75% RH) to incubate for 24 h. Without aerogel (CK), pure aerogel (PCNF), and aerogel with CS (PCNF@CS) were set as controls.

Preservation of fresh pork

The pork used in the experiment was pork loin with the fat removed. On an ultra-clean table, the pork was cut into pieces of uniform appearance and quality along the grain of the pork with 5 g each piece, and divided into three groups. Control group was packed without aerogel liner, treatment group 1 was packed with P3CNF liner, and treatment group 2 was packed with P3CNF@CN liner. Samples were packed in 6 cm × 6 cm polypropylene (PP) trays as containers and wrapped with PE film, respectively, and then stored at 4 °C for 12 days. The L*, a*, pH, and total viable count (TVC) of the pork were determined at regular intervals.

Results and discussion

FT-IR, XRD, and particle size of CS–CN

The FT-IR of CS and CS–CN was shown in Fig. 2(A). The spectrogram of CS shows the maximum absorption peak at 1089 cm^{-1}, which corresponds to the vibrational absorption peak of –OH attached to C-6 in the CS unit (Wu et al., 2016). The peaks at 1630 cm^{-1} and 1597 cm^{-1} corresponds to the stretching vibrational peak of the amide I bond (C=O) and the bending vibrational peak of the amide II bond (N–H) of CS, respectively (Zhu et al., 2023). After the Schiff base

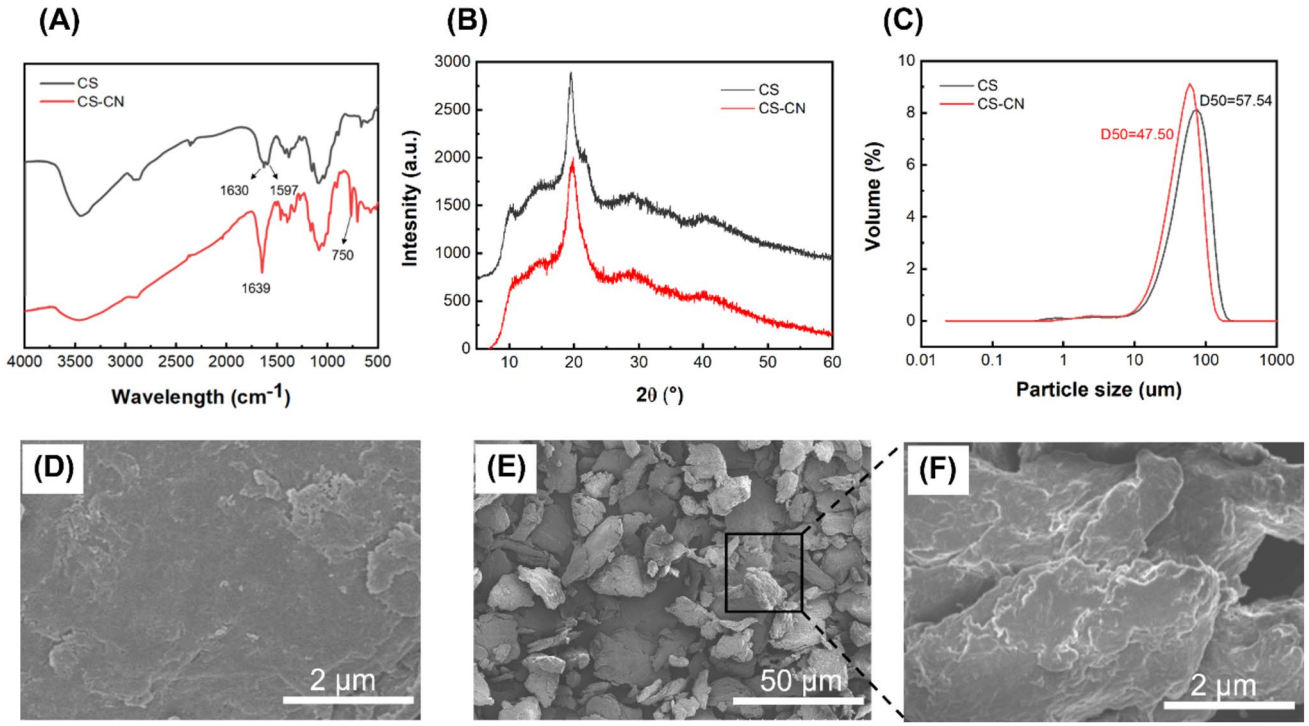

Fig. 2 Characterization of samples. (**A**) FT-IR of CS and CS–CN; (**B**) XRD of CS and CS–CN; (**C**) Particle size of CS and CS–CN; (**D**) SEM of CS; (**E**) SEM of CS–CN; (**F**) SEM of CS–CN

grafting reaction, CS–CN shows a strong absorption band at 1639 cm^{-1} which is caused by the C=N stretching vibration of the formed imine bond. This characteristic peak proves that CN was successfully grafted with CS to form the Schiff base complex (Cionti et al., 2021). Since the grafting reaction consumed the amino group in CS, the absorption peak of N–H in the IR spectrogram of CS–CN was significantly weakened. CS–CN shows the characteristic peak of aromatic aldehyde at 750 cm^{-1}, further indicating the presence of CN in the complex.

As shown in Fig. 2(B), CS is a semi-crystalline polymer with two sharp diffraction peaks at 2θ angles 10.2° and 19.5° and weaker diffraction peaks at 15° and 21.7°. This is due to the strong inter- and intra-molecular hydrogen bonds formed by the amino group of C-2 and the hydroxyl group of C-3 in the CS molecule (Anush et al., 2018). The disappearance of the weak diffraction peak of CS–CN at 10.2° and 21.7° indicates that the molecular chain stacking structure caused by the hydrogen bonding of CS was disrupted by the introduced aldehyde group, which reoriented part of the CS molecular chain and reduced the orderliness of the crystal (Malekshah et al., 2021).

As Fig. 2(C) shows, the D50 particle size of CS–CN is slightly smaller than that of CS due to the destruction of the original crystallinity and spatial barrier introduced by benzene ring after grafting of CN on the shell CS molecular chain, as evidenced by the XRD results.

SEM of CS–CN

The morphology of CS and CS–CN was shown in Fig. 2(D)–(F). The CS surface is smoother and flatter, attributed to the high crystallinity due to the hydroxyl group (Tamer et al., 2023). In contrast, the surface of CS–CN becomes rough and obvious grooves appeared. This was due to the change in the order and internal crystal structure of polymer chains caused by the introduction of aromatic benzene rings, and the appearance of new bonds and reaction sites (Hassan et al., 2018).

Degree of substitution of CS–CN

Since the Schiff base reaction is a substitution reaction of an aldehyde-containing molecule for an amino group and the introduction of a carbon element. Therefore, after the substitution reaction, the C/N of CS–CN is greater than that of CS. The degree of substitution reflects the degree of CS Schiff-base conversion and is numerically equal to the ratio of the total number of moles of C/N in the CS derivatives to the total number of moles of sugar residues in the derivatives. The result of the elemental analysis was shown in Table S1.

UV–Vis spectroscopy

To verify the feasibility of pH-responsive controlled release of CS–CN, the UV–Vis absorption spectra of the raw materials and CS–CN were scanned. As shown in Fig. 3(A), due to the lack of chromophores, CS didn't exhibit strong absorption peaks (Zhu et al., 2023). CN is an aromatic aldehyde, which has both benzene ring structure and carbon–carbon double bond, and can form a ternary conjugated structure with imine bond, so it showed a strong absorption peak at 291 nm (Ni and Yang, 2012). The absorption peak of CS–CN in pH 3 solution is similar to that of CN, indicating that the acid can trigger CN release from CS–CN resulting in an absorption peak at 291 nm.

The UV absorption curves of CS–CN at different pH values are shown in Fig. 3(B). As the pH of the solution decreased from neutral to acidic, the absorption intensity of CS–CN solution at 291 nm gradually improves. This suggested that CS–CN can sense pH changes in the environment and release CN to varying degrees, exhibiting pH-responsive controlled release characteristics.

pH-responsive release and storage stability of CS–CN

The release of CN at different pHs is tested, as shown in Fig. 3(C). Consistent with the UV spectroscopy, the cumulative release of CN and the release rate both increase with decreasing in pH. But in the solution at pH 7 and 9, the imine bond is more stable. The cumulative release of CS–CN is only 10.3% after 72 h of release under neutral conditions. In contrast, in a weak acid buffer solution at pH 5, the release of CN shows a release pattern of rapid release in the early

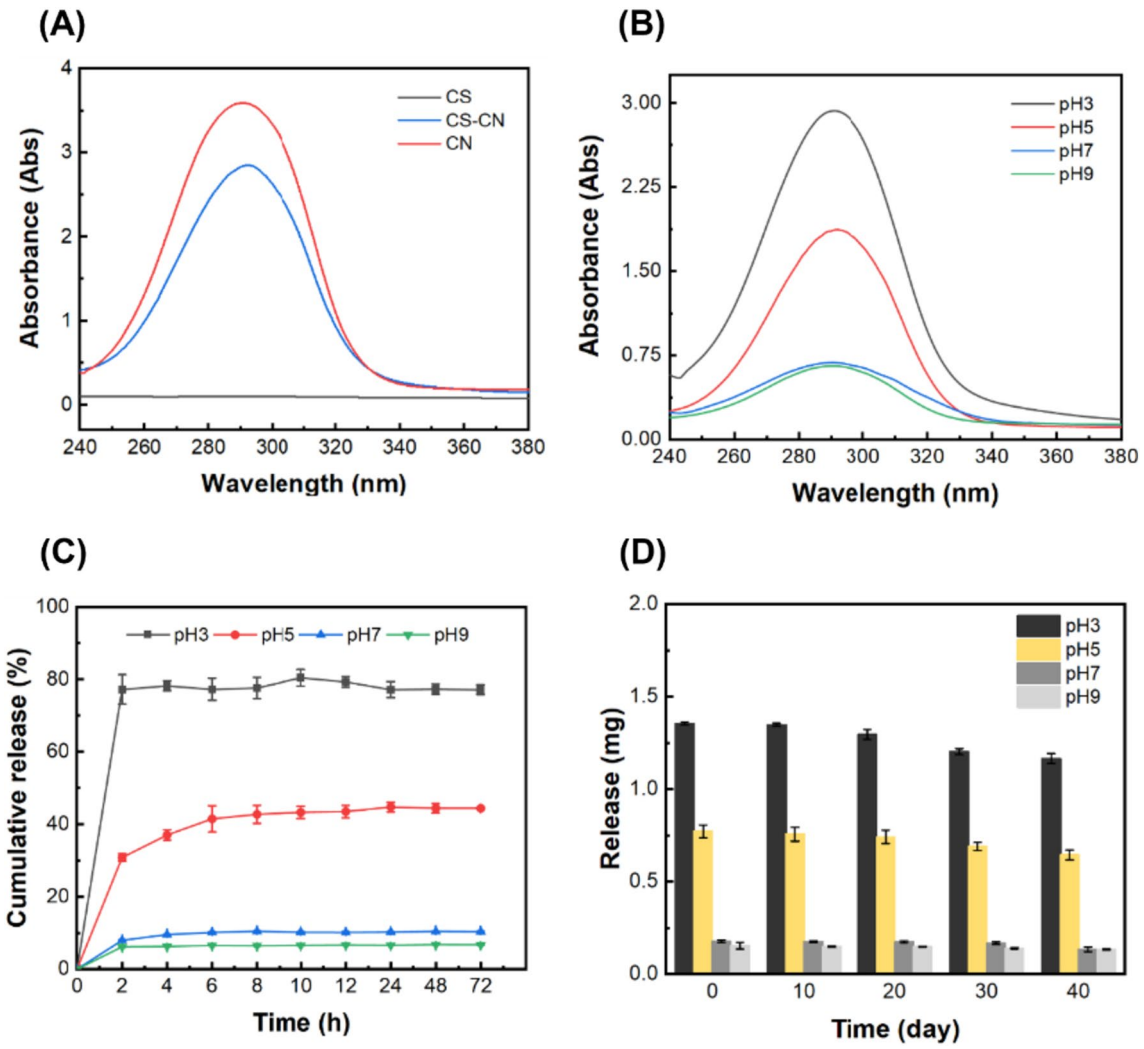

Fig. 3 (**A**) UV–Vis spectroscopy of CS, CN, and CS–CN; (**B**) UV–Vis spectroscopy of CS–CN at different pH; (**C**) CN release from CS–CN under different pH conditions; (**D**) Release stability of CS–CN during 40 days of storage

stage, followed by slow release, which tends to equilibrium at 8 h and reaches 46.18% of cumulative release.

The release rate of CN is the fastest at pH 3, and the cumulative release can reach 77.2% after 2 h. This was due to the easy hydrolysis of imine bonds in acidic systems, and the higher the ambient acidity, the more rapid and complete of the hydrolysis. The analysis in combination with the properties of CS may be related to its residual amine protonation in the solution at pH 3. As CS and the $–NH_2$ re-generated after hydrolysis were protonated to $–NH_3^+$ in the acidic solution, the large number of positive charges repelling each other promoted the stretching of molecular chains (Zhang et al., 2018). Thus, the H^+ could contact with the imine bond more fully, further accelerating the imine bond hydrolysis and released more aldehydes. In addition, the cumulative release of CN in pH 3 solution showed a decreasing trend after reaching the maximum value, and the analysis of the reason may be related to the hydration of α-β unsaturated carbonyl compounds. In acidic environment, aldehydes easily undergo nucleophilic addition reactions with water (Jin and Hanefeld, 2011). As the hydrolysis proceeded, the aldehyde content in the environment increased, and when the hydration rate of aldehyde was greater than the hydrolysis rate of imine bond, it caused a decrease in absorbance.

The storage stability of CS–CN is one of the important properties of its pH response stability and application feasibility. Figure 3(D) reflects the cumulative release of CN from CS–CN after 8 h of release in different pH buffers during 40 days of storage. It can be observed the pH-responsive release of CN is generally stable during the storage period, and the decrease is not significant. The cumulative release at pH 3 and 5 could be maintained between 1.16–1.35 mg and 0.64–0.77 mg, respectively, and with the decreased by 13.9% and 16.5%. In the medium-alkaline condition, the release of CN was reduced by 0.04 mg and 0.02 mg after 40 days. The reduction of release is lower compared to the acidic condition, probably because CS–CN was not sensitive to the non-acidic condition, so the reduction of release was not obvious. CN is a volatile essential oil, and although its volatilization can be reduced by encapsulation, it will still be slowly released into the environment by diffusion to some extent (Wei et al., 2023). The relatively stable release of CS–CN prepared in this paper within 40 days indicated that anchoring CN on the CS surface by grafting could improve its stability and maintain pH-responsive release over a longer period time.

FT-IR of aerogel

The FT-IR of aerogels was shown in Fig. 4(A). CNF has a large energy band at 3328 cm^{-1} due to the stretching vibration of –OH. Besides, a strong absorption peak at 1607 cm^{-1} can be observed, attributed to the carbonyl characteristic peak of the carboxyl group (Zhao et al., 2022). Compared to CNF, the absorption peak of PCNF at 1706 cm^{-1} may be related to the residual carboxyl group of CNF, and it is reduced and red-shifted due to intermolecular hydrogen bonding (Zhou et al., 2022). The absorption peak at 850 cm^{-1} is characteristic of PVA, which is in agreement with the results of Takeno et al. (2020). After loading CS–CN, PCNF@CN shows a new peak at 1629 cm^{-1} with an offset from the peak wave number of CS–CN. It may be an overlapping peak caused by the stretching vibration of C=N and the bending vibration of the CS amide bond (Si et al., 2021). The presence of this absorption peak proves that CS–CN has been successfully loaded in the aerogel.

Morphologies and structural characteristics of aerogels

As displayed in Fig. 4(B) (a–f), all aerogels show porous network structures. The aerogel without CS–CN can be observed more membrane-like structure on its surface [Fig. 4(B) (a)], which may be due to the inter- and intramolecular linkage entanglement of CNF and PVA through hydrogen bonding and the sublimation of crystalline ice under vacuum to form larger membranes (Xu et al., 2021). In contrast, the addition of CS–CN resulted in the disappearance of the lamellar film structure and the formation of a highly interconnected and unevenly oriented open-hole microstructure.

The pore size of the aerogel decreases with increasing PVA content and a more ordered pore distribution is formed [Fig. 4(B) (b)–(e)]. The pore structure of P5CNF@CN aerogel is the most uniform and dense, and CS–CN can be clearly seen attached and wrapped in the three-dimensional network structure [Fig. 4(B) (e)]. As shown in Fig. 4(B) (f), the distribution of CS–CN is more easily observed due to the smaller pore size of P5CNF@CN, where part of the CS–CN seals the pores.

Figure S1(B) shows the porosity and density of aerogels prepared with different PVA contents. The porosity of pure CNF was 92.15%, and with the increase of PVA content, the porosity showed a trend of increasing and then decreasing, and reached a maximum porosity of 98.07%, which was attributed to the fact that the addition of PVA could make the aerogel form a denser and more regular pore structure. And with the continued increase of PVA, the porosity decreased to 95.94%, which on the one hand, maybe due to the collapse and blockage of some micropores of the aerogel caused by physical cross-linking (Zhang et al., 2021). On the other hand, the smaller pore size of P5CNF@CN and the blocking of some of the pores by CS–CN, as shown in SEM, led to a decrease in the porosity of the aerogel. The higher porosity of aerogels helps to promote the loading and controlled

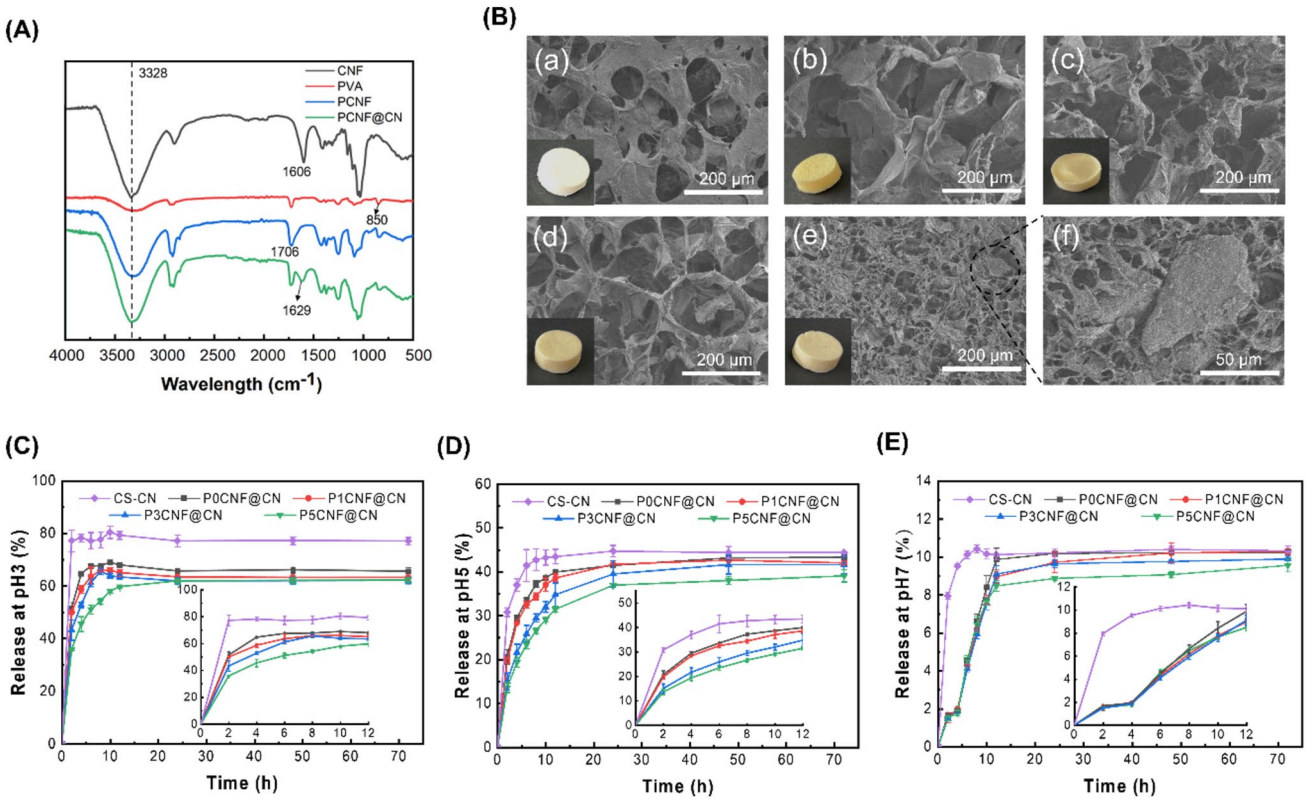

Fig. 4 Characterization of samples. (**A**) FT-TR of aerogels; (**B**) SEM of samples. (a)–(f) SEM of P3CNF without CS–CN, P0CNF@CN; P1CNF@CN; P3CNF@CN; P5CNF@CN, respectively; (**C**)–(**E**) Cumulative release curve of CN from CS–CN and PCNF@CN aerogels at pH 3, pH 5, and pH 7

release of actives, which is important for antimicrobial packaging and delivery of active agents in the food field.

The density of the aerogels increased significantly from 37.75 to 54.8 mg/cm^3 with the increase of PVA content, which was attributed to the more PVA linking and entangling with CS through hydrogen bonding, forming a more stable three-dimensional network structure.

Mechanical properties of aerogel

In packaging applications, the greater load-bearing capacity of aerogel can provide protection against mechanical stresses on the product during transportation or handling. As Fig. S1(A) shows, the stress–strain curve profile has three stages. In the initial stage, when the aerogel is under slight pressure, the material is in elastic deformation and the compressive strain is around 10%. In the middle stage, the aerogel pore wall starts to bend, and the curve grows at a relatively slow rate. When the compressive deformation exceeds a certain value, most of the air in the aerogel is extruded, and the volume is continuously reduced and accompanied by the plugging of pores and collapse of pores. At the time, the porous structure of the aerogel was completely destroyed with the stress increasing rapidly (Wang et al., 2024).

The compressive strength and compressive modulus of aerogels are closely related to the microstructure. With the increase of PVA content, the compression modulus and compression strength of aerogels showed a rising trend, which was related to the increase of the interaction sites between the molecules of the aerogel skeleton. The cross-linked network structure of the aerogels is not only formed by PVA but also by the physical cross-linking of carboxyl groups and residual –OH of CNF (Si et al., 2021). In the mixed system, PVA acts as the continuous phase while CNF acts as the dispersed phase. After hydrogen bonding cross-linking, CNF is dispersed in PVA and serves as the scaffold for the entire aerogel structure, while PVA acts as the reinforcing material, forming an interpenetrating network structure and reducing the pore size of the aerogel, which is consistent with SEM results (Ahmad et al., 2022). When the PVA content is low, the pore size of the aerogel is relatively large. After external compression, the mutual support between the large pores is weaker than that of the small pores, making it difficult to effectively transmit and disperse external forces. Additionally, air is more likely to escape from larger pores, resulting in lower compressive strength and compressive modulus (Lin and Jana, 2021).

pH-responsive release of CN from aerogels

The release of CN from CS–CN and CNF/PVA aerogels at different pH was tested. It shows that the aerogel still had pH-responsive release properties [Fig. 4(C)–(E)]. The release process of CN is closely related to moisture. In a high humidity environment, moisture breaks the hydrogen bonds between cellulose chains and the aerogel absorbs water. CS–CN is stimulated by pH to undergo the Schiff base hydrolysis reaction and relies on the concentration difference to diffuse outward.

As shown in Fig. 4(C), P1CNF@CN and P3CNF@CN reached the release equilibrium at 8 h with a cumulative release of 65.8% and 65.6%, respectively, which delayed the release time by 6 h compared to the CS–CN. In addition, P5CNF@CN is the most effective in slowing release rate, and the equilibrium release time can be extended to 24 h. It is because the porous structure of the aerogel makes the diffusion path of CN within the cellulose network longer. –COOH and residual –OH of CNF fibers combined with the –OH of PVA molecules to form hydrogen bonds, and interacted to form a cross network, which reduced the pore size of the aerogel (Ahmad et al., 2022). And with the increase of PVA, the physical entanglement between cellulose and PVA molecules was enhanced, which reduced the mobility of polymer molecular chains and the extent of water molecules entering inside the polymer through the amorphous region (Xu et al., 2021), making the release path of CN more circuitous.

The release rate and cumulative release of CN are slightly lower in pH 5 than in pH 3. These results demonstrated that the CN release rate was not only influenced by the pore size of the aerogel, but also related to the acidity of the release environment. It is also noteworthy that the cumulative release at the equilibrium of aerogel is lower than that of CS–CN. This could be due to the capillary pressure generated when porous material is immersed in liquid, causing volume contraction and collapse of the internal micropores of the aerogel, which in turn leads to pore blockage and hindrance in the release of CN (Lin and Jana, 2021).

The release curve of CN under neutral conditions was different. The cumulative release is about 1.8% in the first 2 h, while it increases slightly from 2 to 4 h. This may be due to the hydrolysis of CS–CN attached to the aerogel surface in the first 2 h. And as the release proceeds, –COOH was deprotonated in neutral solution, which reduced the hydrogen bonding with PVA, and the $–COO^-$ repelled each other, increasing the gap between polymer molecular chains and promoting the formation of hydrogen bonds between water and PVA, thus accelerating the hydrolysis of Schiff base (Bhandari et al., 2017).

Release kinetic analysis

Three common release kinetic models, including the first-order model, the Higuchi model, and the Korsmyer–Peppas model (Jabbari-Gargari et al., 2022), were chosen to study the kinetics of CN release from PCNF@CN at pH 3 and 5.

As Fig. S2 and Table S2 show, both the first-order kinetic model and Korsmyer-Peppas can fit the release data of CN in the pH 3 and 5 well. Good correlation coefficient (R^2) indicates that the release rate of CN is proportional to time. As for aerogels, all three kinetic models can fit the release of CN better under all conditions (R^2 is greater than 0.95), except for the pH 3 condition, where the Higuchi model cannot be fitted well.

After loading CS–CN into aerogels, the release rates k fitted by all three models were smaller than those of CS–CN. And the k decreased with the increase of PVA, indicating that adjusting the pore size and microstructure of aerogels could control the release rate of CN. In addition, the k of CN in pH 3 was significantly higher than that in pH 5 for both pure CS–CN and aerogels, further demonstrating that the hydrolysis rate of imine bonds was related to the environmental acidity.

The parameter n in the Korsmeyer–Peppas model can reflect the release mechanism of the aerogel carrier releasing the active substance. As the parameter n in Table S2 shows, the release mechanism of CNF/PVA aerogel in pH 3 is Fick diffusion and CN mainly relies on the concentration difference for release. The parameter n in pH 5 buffer varied from 0.3416 to 0.4564, indicating that the mechanism of CN release from CNF/PVA changed from Fick diffusion to non-Fick diffusion with the increase of PVA. It is probably because PVA contains many hydroxyl groups, which are highly hydrophilic. As the release proceeds, the aerogel can adsorb more water molecules. Therefore, the release of CN was affected by a combination of diffusion and swelling of the aerogel skeleton (Jabbari-Gargari et al., 2022).

Antimicrobial effect of aerogels

The antibacterial effects of aerogels with CS or CS–CN as well as pure aerogels were shown in Fig. 5. Compared with the CK, the antibacterial effect of PCNF aerogel was not obvious, meanwhile, the addition of CS–CN showed a significant increase in the antibacterial effect in comparison with the aerogel with CS. The antibacterial property of CS lies in the pronated amino groups on the molecule chain can interact with the negative charge on the surface of the bacterial cell membrane to achieve antibacterial by destroying the cell structure (Lee et al., 2023). However, the antimicrobial effect of CS is limited and can't exert the antimicrobial effect brought about by diffusion and migration, and microorganisms are inhibited only after contact with

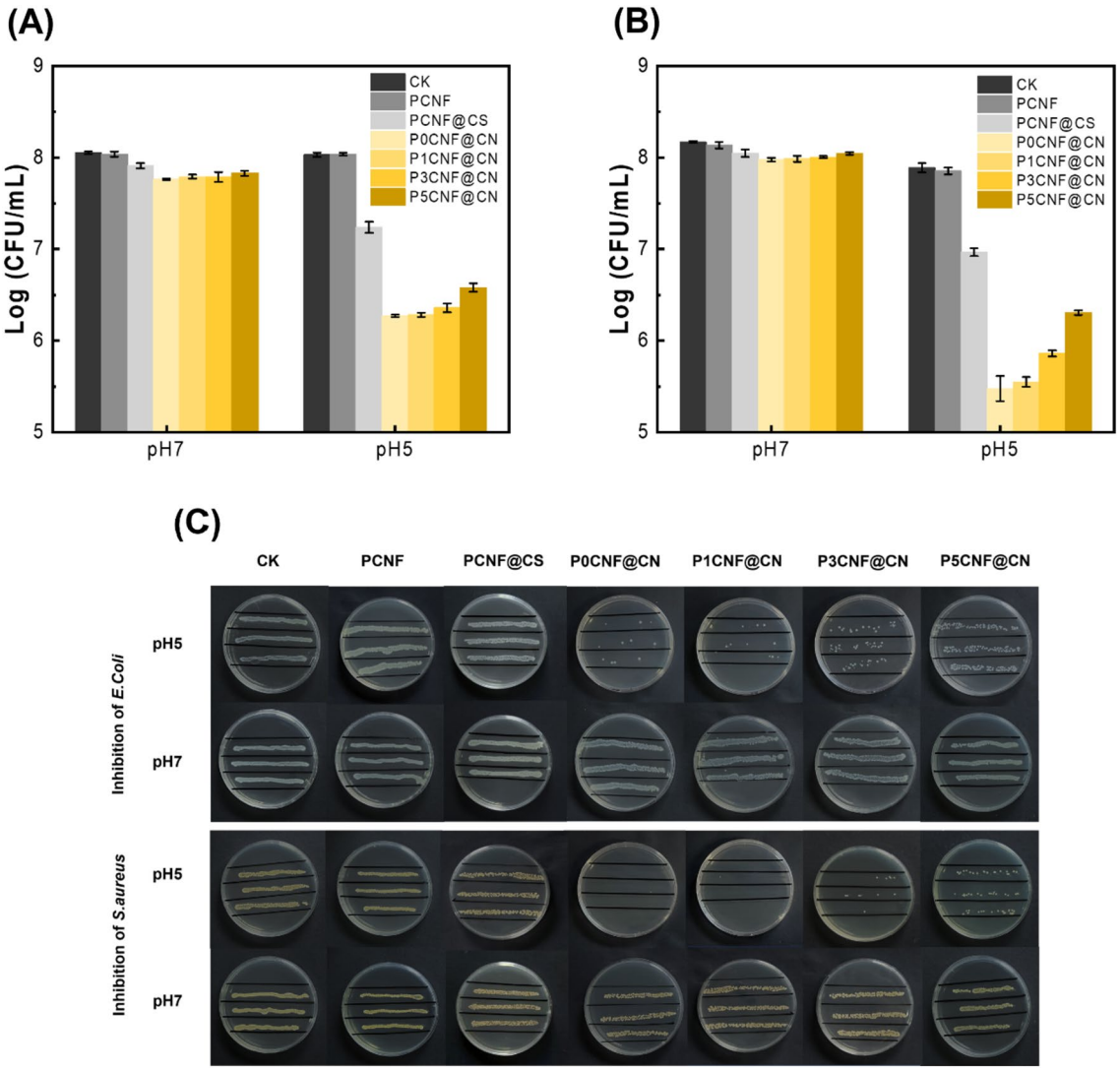

Fig. 5 Antimicrobial effects of samples. (**A**) Antimicrobial effects of different aerogels against *E. coli* at pH 5 and pH 7; (**B**) Antimicrobial effects of different aerogels against *S. aureus* at pH 5 and pH 7; (**C**) Photos of colonies

it (Rodríguez-Núñez et al., 2012). In comparison, the antimicrobial effect of aerogels with CS–CN was better. Under acidic conditions at pH 5, the imine bond was hydrolyzed. The aerogels has stronger antibacterial properties with the dual effect of amino protonation and release of CN. The aldehyde group of CN is a nucleophilic group, which is easily adsorbed by the hydrophilic groups on the bacterial surface. CN has obvious bactericidal effect by destroying the integrity of the cell wall, affecting the synthesis of enzymes and proteins and thus inhibiting the growth of microorganisms (Ooi et al., 2006). At pH 7, on the other hand, the aerogel showed only a slight inhibitory effect due to the low protonation of amino and the stabilization of the imine bond.

Besides, there were some differences in the antibacterial effect of aerogels. The bacteriostatic ability of aerogels against *E. coli* and *S. aureus* decreased with increasing PVA. This was attributed to PVA forming a dense network structure with cellulose through hydrogen bonding, which limited the diffusion of CN around the pores, thus reducing the antimicrobial activity of the aerogel. P5CNF@CN showed the lowest antimicrobial effect, which may be due to its own small pore size that delayed the release of CN on the one hand; on the other hand, the capillary pressure generated when the aerogel absorbed moisture and caused the collapse of the tiny pores inside the aerogel, which led to the blockage and closure of the pores and impeded the release of CN. In addition, the aerogel loaded with CS–CN had a greater limiting effect on *S. aureus* than on *E. coli*. Compared with the control (CK), the count of *E. coli* and *S. aureus* decreased by 1.78 log CFU/mL and 2.41 log CFU/mL, respectively, which indicated that *S. aureus* was more sensitive to CN. As a Gram-positive bacterium, *S. aureus*

cell wall is mainly composed of porous peptidoglycan, which lacks the protection of the outer membrane as well as the enzymes in the periplasmic space, so CN is more likely to penetrate and damage the cell wall (Wang et al., 2022a). In contrast, *E. coli*, as a Gram-negative bacterium, has a less negatively charged cell surface and a higher content of lipopolysaccharide in the outer membrane, which can block the entry of antibacterial agents (Shen et al., 2015; Zhang et al., 2016).

Preservation of fresh pork by antimicrobial aerogel pads

Based on the previous mechanical and antimicrobial tests, P3CNF@CN aerogel exhibits optimal performance comprehensively. Thus, fresh pork was preserved with P3CNF@CN. Color is one of the most important quality indicators of fresh meat. The appearance and color of pork in each group are shown in Figs. 6(A) and S3. After 12 days of storage, the pork in the control group had a dark color, a sticky surface, and emitted an unpleasant smell. The L* and a* of all the meat showed a decreasing trend over 12 days. Compared with the control group, the decrease of L* and a* of fresh meat with aerogel pads could be controlled, especially for the pork samples with CS–CN added. It suggests that the juice exuded from fresh pork during storage triggered the release of CN and the aerogel mat could improve the bacterial inhibition and delay the color decline by absorbing water and releasing antimicrobial agents.

The pH of fresh pork was shown in Fig. 6(B). There is a decrease in pH after 2 days due to the decomposition of muscle glycogen to produce lactic acid. And as microorganisms multiplied on the meat surface, proteins were broken down to produce substances such as biogenic amines, resulting in a continuous rise in pH (Wang et al., 2024). The pH of the control group rose significantly faster than that of the aerogel-packed fresh pork, and the pH of the control group was 6.33 after 6 days, which was in the secondary freshness state ($6.2 < pH < 6.4$), whereas that of the experimental group was 6.01 and 5.73, respectively. This was attributed to the fact that the aerogel absorbed the juices of the pork and suppressed the growth of microorganisms and slowed down the deterioration of the meat.

Spoilage of fresh pork is mainly caused by microorganisms. The total viable counts (TVC) of fresh pork in all groups over 12 days were shown in Fig. 6(C). The TVC of fresh pork in all groups increased with the time. During the early period, the TVC of fresh pork in the P3CNF@CN group increased slowly, which was attributed to the release of CN triggered by the absorption of exuded juices from

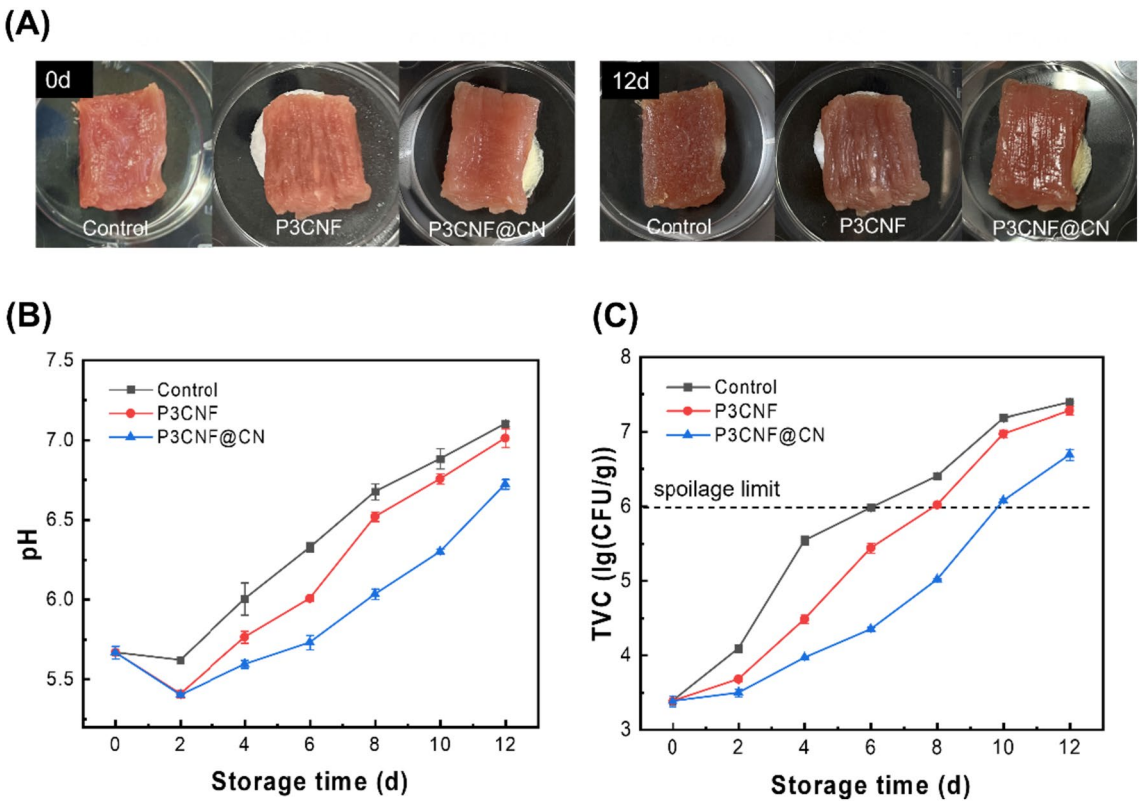

Fig. 6 (**A**) Appearance of meat before and after storage; (**B**) pH; (**C**) Total viable count (TVC)

the fresh pork by the aerogel, and then significantly inhibited microbial growth in the initial period. Referring to the standard GB/T 17238-2008, the TVC of the control group reached 5.98 lg CFU/g after 6 days, which was close to the spoilage limit value of 6.0 lg CFU/g (Chen et al., 2022). And it increased to 6.4 lg CFU/g after 8 days, which was beyond the limit and the fresh pork was spoiled. In contrast, the meat with aerogel pads had significantly lower TVC than the control group and exceeded the standard upper limit after 8 and 10 days, respectively. These results showed that P3CNF@CN had a good preservation effect on fresh pork and could prolong the shelf-life of fresh pork for about 4 days.

In conclusion, CS–CN containing a pH-responsive switch was synthesized in this paper by a one-pot method with facile preparation conditions. Imine bonding had improved the stability of CN, which could anchor the volatile antimicrobial agent to the polymer in a longer period of time until it was triggered by the acidic pH when it was needed to be released. The CNF/PVA aerogel with CS–CN added has good antimicrobial properties and the gradual release of CN can be achieved by utilizing the porous structure of the aerogel. In addition, attributed to the hydrolysis of C=N, the aerogels showed significant pH-responsive differences in bacterial inhibition against *E. coli* and *S. aureus*, with the highest reductions of 1.78 log CFU/mL and 2.41 log CFU/mL, respectively. The P3CNF@CN with the optional comprehensive performance was used in the preservation of fresh pork, and the shelf life could be delayed for about 4 days by taking advantage of the water-absorbency of the aerogel and triggered the release of CN. Therefore, The CNF/PVA-based aerogel can be used as a delivery carrier for pH-responsive complexes to develop an environmentally responsive food antimicrobial packaging system with targeted delivery and intelligent release.

Supplementary Information The online version contains supplementary material available at https://doi.org/10.1007/s10068-023-01487-8.

Acknowledgements This work is supported by Fundamental Scientific Research Funds of Central Universities (JUSRP21115); Independent Research Project Funding Project of Jiangsu Key Laboratory of Advanced Food Manufacturing Equipment Technology (FMZ201902); Postgraduate Research & Practice Innovation Program of Jiangsu Province (1072050205238200); Postgraduate Research & Practice Innovation Program of Jiangsu Province (1075212042230360).

Author contributions TH: investigation and writing of manuscript. FW: conceptualization and validation. LW: project administration, writing—review and editing. All authors reviewed and commented on manuscript.

Declarations

Conflict of interest The authors declare no conflicts of interest.

References

Ahmad H, Anguilano L, Fan M. Microstructural architecture and mechanical properties of empowered cellulose-based aerogel composites via TEMPO-free oxidation. Carbohydrate Polymers. 298: 120117 (2022)

Anush SM, Vishalakshi B, Kalluraya B, Manju N. Synthesis of pyrazole-based Schiff bases of chitosan: evaluation of antimicrobial activity. International Journal of Biological Macromolecules. 119: 446-452 (2018)

Bhandari J, Mishra H, Mishra PK, Wimmer R, Ahmad FJ, Talegaonkar S. Cellulose nanofiber aerogel as a promising biomaterial for customized oral drug delivery. International Journal of Nanomedicine. 12: 2021-2031 (2017)

Chabbi J, Aqil A, Katir N, Vertruyen B, Jerôme C, Lahcini M, El Kadib A. Aldehyde-conjugated chitosan-graphene oxide glucodynamers: ternary cooperative assembly and controlled chemical release. Carbohydrate Polymers. 230: 115634 (2020)

Chen L, Niu X, Fan X, Liu Y, Yang J, Xu X, Zhou G, Zhu B, Ullah N, Feng X. Highly absorbent antibacterial chitosan-based aerogels for shelf-life extension of fresh pork. Food Control. 136: 108644 (2022)

Cionti C, Taroni T, Sabatini V, Meroni D. Nanostructured oxide-based systems for the pH-triggered release of cinnamaldehyde. Materials. 14: 1536 (2021)

Cui H, Cheng Q, Li C, Khin MN, Lin L. Schiff base cross-linked dialdehyde β-cyclodextrin/gelatin-carrageenan active packaging film for the application of carvacrol on ready-to-eat foods. Food Hydrocolloids. 141: 108744 (2023)

Hassan MA, Omer AM, Abbas E, Baset WMA, Tamer TM. Preparation, physicochemical characterization and antimicrobial activities of novel two phenolic chitosan Schiff base derivatives. Scientific Reports. 8: 11416 (2018)

Heras-Mozos R, Gavara R, Hernández-Muñoz P. Responsive packaging based on imine-chitosan films for extending the shelf-life of refrigerated fresh-cut pineapple. Food Hydrocolloids. 133: 107968 (2022)

Jabbari-Gargari A, Moghaddas J, Jafarizadeh-Malmiri H, Hamishehkar H. Ambient pressure drug loading on trimethylchlorosilane silylated silica aerogel in aspirin controlled-release system. Chemical Engineering Communications. 209: 1612-1625 (2022)

Jin J, Hanefeld U. The selective addition of water to CC bonds; enzymes are the best chemists. Chemical Communications. 47: 2502-2510 (2011)

Jose J, Pai AR, Gopakumar DA, Dalvi Y, Ruby V, Bhat SG, Pasquini D, Kalarikkal N, Thomas S. Novel 3D porous aerogels engineered at nano scale from cellulose nano fibers and curcumin: an effective treatment for chronic wounds. Carbohydrate Polymers. 287: 119338 (2022)

Lee S, Kim S, Bang W, Yuk H. Combined antibacterial effect of 460 nm light-emitting diode illumination and chitosan against *Escherichia coli* O157:H7, *Salmonella* spp. and *Listeria monocytogenes* on fresh-cut melon, and the impact of combined treatment on fruit quality. Food Science and Biotechnology. (2023) https://doi.org/10.1007/s10068-023-01324-y.

Lin W-H, Jana SC. Analysis of porous structures of cellulose aerogel monoliths and microparticles. Microporous and Mesoporous Materials. 310: 110625 (2021)

Long L-Y, Weng Y-X, Wang Y-Z. Cellulose aerogels: synthesis, applications, and prospects. Polymers. 10: 623 (2018)

Malekshah RE, Shakeri F, Aallaei M, Hemati M, Khaleghian A. Biological evaluation, proposed molecular mechanism through docking and molecular dynamic simulation of derivatives of chitosan. International Journal of Biological Macromolecules. 166: 948-966 (2021)

Meng Q, Xue Z, Chen S, Wu M, Lu P. Smart antimicrobial Pickering emulsion stabilized by pH-responsive cellulose-based nanoparticles. International Journal of Biological Macromolecules. 233: 123516 (2023)

Ni L, Yang X. Determination of cinnamaldehyde and piperine in Shiliu Jianwei pill by HPLC. Chinese Journal of Modern Applied Pharmacy. 29: 67-69 (2012)

Ooi L, Li Y, Kam S, Wang H, Wong E, Ooi V. Antimicrobial activities of cinnamon oil and cinnamaldehyde from the Chinese medicinal herb *Cinnamomum cassia* Blume. American Journal of Chinese Medicine. 34: 511-522 (2006)

Rincón E, Espinosa E, Pinillos M, Serrano L. Bioactive absorbent chitosan aerogels reinforced with bay tree pruning waste nanocellulose with antioxidant properties for burger meat preservation. Polymers. 15: 866 (2023)

Rodríguez-Núñez JR, López-Cervantes J, Sánchez-Machado DI, Ramírez-Wong B, Torres-Chavez P, Cortez-Rocha MO. Antimicrobial activity of chitosan-based films against *Salmonella typhimurium* and *Staphylococcus aureus*. International Journal of Food Science & Technology. 47: 2127-2133 (2012)

Shen S, Zhang T, Yuan Y, Lin S, Xu J, Ye H. Effects of cinnamaldehyde on *Escherichia coli* and *Staphylococcus aureus* membrane. Food Control. 47: 196-202 (2015)

Si R, Wu C, Yu D, Ding Q, Li R. Novel TEMPO-oxidized cellulose nanofiber/polyvinyl alcohol/polyethyleneimine nanoparticles for Cu^{2+} removal in water. Cellulose. 28: 10999-11011 (2021)

Takeno H, Inoguchi H, Hsieh W-C. Mechanical and structural properties of cellulose nanofiber/poly(vinyl alcohol) hydrogels crosslinked by a freezing/thawing method and borax. Cellulose. 27: 4373-4387 (2020)

Tamer TM, ElTantawy MM, Brussevich A, Nebalueva A, Novikov A, Moskalenko IV, Abu-Serie MM, Hassan MA, Ulasevich S, Skorb EV. Functionalization of chitosan with poly aromatic hydroxyl molecules for improving its antibacterial and antioxidant properties: practical and theoretical studies. International Journal of Biological Macromolecules. 234: 123687 (2023)

Valero A, Pérez-Rodríguez F, Carrasco E, Fuentes-Alventosa JM, García-Gimeno RM, Zurera G. Modelling the growth boundaries of *Staphylococcus aureus*: effect of temperature, pH and water activity. International Journal of Food Microbiology. 133: 186-194 (2009)

Wang S, Wang F, Lu C, Ma S, Gu Y, Wang L. Citral-loaded nanocellulose/sodium alginate aerogel packaging liner for fresh pork preservation. Food Control. 155: 110031 (2024)

Wang L, Xu J, Zhang M, Zheng H, Li L. Preservation of soy protein-based meat analogues by using PLA/PBAT antimicrobial packaging film. Food Chemistry. 380: 132022 (2022a)

Wang P, Zou Y, Li Y, Qin Z, Liu X, Zhang H. pH-sensitive self-assembled nanofibers based on electrostatic interaction and Schiff base bonding for controlled release of curcumin. Food Hydrocolloids. 131: 107805 (2022b)

Wei C, Fan C, Xie D, Zhou S, Zhang H, Du Q, Jin P. Fabrication of cinnamaldehyde-entrapped ethosome nanoparticles as antimicrobial agent. LWT 181: 114760 (2023)

Wu W. Facile fabrication of multifunctional citrus pectin aerogel fortified with cellulose nanofiber as controlled packaging of edible fungi. Food Chemistry. 374: 131763 (2022)

Wu C, Wang L, Fang Z, Hu Y, Chen S, Sugawara T, Ye X. The effect of the molecular architecture on the antioxidant properties of chitosan gallate. Marine Drugs. 14: 95 (2016)

Xu J, Liu Y, Hsu S. Hydrogels based on Schiff base linkages for biomedical applications. Molecules. 24: 3005 (2019)

Xu J, Song W, Wu N, Tong J, Ren L. Preparation and characterization of chitosan/polyvinyl porous alcohol aerogel microspheres with stable physicochemical properties. International Journal of Biological Macromolecules. 187: 614-623 (2021)

Zhang Z, He C, Chen X. Hydrogels based on pH-responsive reversible carbon–nitrogen double-bond linkages for biomedical applications. Materials Chemistry Frontiers. 2: 1765-1778 (2018)

Zhang Y, Liu X, Wang Y, Jiang P, Quek S. Antibacterial activity and mechanism of cinnamon essential oil against *Escherichia coli* and *Staphylococcus aureus*. Food Control 59: 282-289 (2016)

Zhang A, Zou Y, Xi Y, Wang P, Zhang Y, Wu L, Zhang H. Fabrication and characterization of bamboo shoot cellulose/sodium alginate composite aerogels for sustained release of curcumin. International Journal of Biological Macromolecules. 192: 904-912 (2021)

Zhao R, E S, Ning D, Ma Q, Geng B, Lu Z. Strengthening and toughening of TEMPO-oxidized cellulose nanofibers/polymers composite films based on hydrogen bonding interactions. Composites Communications. 35: 101322 (2022)

Zhou T, Cheng X, Pan Y, Li C, Gong L. Mechanical performance and thermal stability of polyvinyl alcohol–cellulose aerogels by freeze drying. Cellulose. 26: 1747-1755 (2019)

Zhou Z, Yao Y, Zhang J, Shen L, Xu H, Liu J, Shentu B. Effects of poly(vinyl alcohol) (PVA) concentration on rheological behavior of TEMPO-mediated oxidized cellulose nanofiber/PVA suspensions. Cellulose. 29: 8255-8263 (2022)

Zhu J, Huang T, Chen X, Tian D, Wang L, Gao R. Preparation and characterization of vanillin-conjugated chitosan-stabilized emulsions via a Schiff-base reaction. Food Science and Biotechnology. (2023) https://doi.org/10.1007/s10068-023-01277-2.